

The ρ^0 and Drell-Söding contributions to central exclusive production of $\pi^+\pi^-$ pairs in proton-proton collisions at high energies

Piotr Lebiedowicz,^a Otto Nachtmann^b and Antoni Szczurek^{a,1}

^a*Institute of Nuclear Physics PAN, PL-31-342 Kraków, Poland*

^b*Institut für Theoretische Physik, Universität Heidelberg,
Philosophenweg 16, D-69120 Heidelberg, Germany*

E-mail: Piotr.Lebiedowicz@ifj.edu.pl,

O.Nachtmann@thphys.uni-heidelberg.de, Antoni.Szczurek@ifj.edu.pl

ABSTRACT: We present a study of the central exclusive $\pi^+\pi^-$ production via the photoproduction mechanism in nucleon-nucleon collisions. The photon-pomeron/reggeon and pomeron/reggeon-photon exchanges both for the ρ^0 resonance contribution and the Drell-Söding contribution are considered. The amplitudes for the processes are formulated in terms of vertices respecting the standard crossing and charge-conjugation relations of Quantum Field Theory. The coupling parameters of tensor pomeron and reggeon exchanges are fixed based on the H1 and ZEUS experimental data for the $\gamma p \rightarrow \rho^0 p$ reaction. We present first predictions of this mechanism for the $pp \rightarrow pp\pi^+\pi^-$ reaction being studied at COMPASS, RHIC, Tevatron, and LHC. We show the influence of the experimental cuts on the integrated cross section and on various differential distributions for outgoing particles. Distributions in rapidities and transverse momenta of outgoing protons and pions as well as correlations in azimuthal angle between them are presented. We compare the photoproduction contribution to $\pi^+\pi^-$ distributions with double pomeron/reggeon two-pion continuum. We discuss whether the high-energy central production of ρ^0 mesons could be selected experimentally.

KEYWORDS: Phenomenological Models

¹Also at Rzeszów University, PL-35-959 Rzeszów, Poland.

Contents

1	Introduction	1
2	Photoproduction of ρ^0 meson	3
3	The central exclusive two-pion production	7
3.1	ρ^0 -resonance contribution	7
3.2	Drell-Söding contribution	9
3.3	Absorptive corrections	11
4	Results	11
5	Conclusions and Outlook	16

1 Introduction

There is a growing interest in understanding the mechanism of exclusive ρ^0 resonance and continuum $\pi^+\pi^-$ production in the nucleon-nucleon collisions. This is closely related to ongoing experimental studies of the COMPASS [1], STAR [2, 3], CDF [4, 5], ALICE [6, 7], ATLAS [8] and CMS [9, 10] collaborations.

Some time ago two of us proposed a simple Regge-like model for the $\pi^+\pi^-$ continuum based on the exchange of two pomerons/reggeons [11]. For further work see [12]. These model studies were extended also to K^+K^- production [13]. Predictions for experiments at different energies have been presented also in Chapter 2 of [14] in order to make precise comparison between calculations and experimental data. In addition to the continuum one has to include also two-pion resonances. Production of scalar and pseudoscalar resonances was studied by us very recently [15] in the context of the theoretical concept of tensor pomeron proposed in Ref. [16]. In the present paper we focus on exclusive production of the ρ^0 resonance followed by the decay $\rho^0 \rightarrow \pi^+\pi^-$. Due to its quantum numbers this resonance state cannot be produced by pomeron-pomeron fusion. The exchanges contributing are photon-pomeron/reggeon and reggeon-pomeron/reggeon.

The $\gamma p \rightarrow \pi^+\pi^-p$ process has been discussed recently [17, 18] within the model for tensor-pomeron and vector-odderon [16]. It was known for a long time that the shape of the ρ^0 in photoproduction is skewed. An explanation was given by Söding following a suggestion by Drell [19–21]; see also [22]. The skewing is due to the interference of continuum $\pi^+\pi^-$ production with the $\pi^+\pi^-$ production through the ρ^0 meson. Usually there are problems of gauge invariance when adding these two contributions to the $\pi^+\pi^-$ production and restoration of the gauge invariance is to some extent arbitrary. The authors of Ref. [17] obtained a gauge-invariant version of the Drell-Söding mechanism which produces

the skewing of the ρ^0 -meson shape. The $\gamma p \rightarrow \pi^+ \pi^- p$ reaction would be helpful to test the model and its parameters against available data.

In the literature exist some phenomenological models of light vector meson photoproduction in the $pp \rightarrow pVp$ reaction, e.g. the color dipole approach [23, 24], and the pQCD k_t -factorization approach [25–28]. In the latter case the authors also consider absorption effects due to strong proton-proton interactions.

In this paper we focus on the four-body $pp \rightarrow pp\pi^+\pi^-$ reaction with the pion pair produced by photon-pomeron/reggeon fusion. For the ρ^0 resonance production we consider the diagrams shown in Fig. 1. In these diagrams all vertices and propagators will be taken here according to Ref. [16]. The diagrams to be considered for the dominant non-resonant (Drell-Söding) contribution are shown in Fig. 2. In the following we collect formulae for the amplitudes for the $pp \rightarrow pp\pi^+\pi^-$ (or $p\bar{p} \rightarrow p\bar{p}\pi^+\pi^-$) reaction within the tensor pomeron model [16]. We expect that the central exclusive ρ^0 photoproduction and its subsequent decay are the main source of P -wave in the $\pi^+\pi^-$ channel in contrast to even waves populated in double-pomeron/reggeon processes.

A complete calculation for central exclusive $\pi^+\pi^-$ production in pp collisions at high energies clearly must take into account more diagrams than those of Figs. 1 and 2. For instance, in these figures we could replace the virtual photon by the ρ_R reggeon. As already mentioned, we can have double pomeron/reggeon exchange leading to $\pi^+\pi^-$ in the continuum or to the $f_2(1270)$ resonance decaying to $\pi^+\pi^-$. We shall come back to all these processes in a further publication. Here we concentrate on our first “building block” for this program, the processes of Figs. 1 and 2. Due to the photon propagators occurring in these diagrams we expect these processes to be most important when at least one of the protons is undergoing only a very small momentum transfer.

There is also a non-central diffractive ρ^0 production via the bremsstrahlung-type mechanism. But the ρ^0 mesons originating from such a mechanism are expected to be produced very forward or very backward in analogy to the ω -bremsstrahlung considered in Ref. [27]. Similar processes were discussed at high energies also for the exclusive π^0 meson [29], and γ [30] production.

Our paper is organised as follows. In section 2 we discuss the $\gamma p \rightarrow \rho^0 p$ reaction. Turning to the $pp \rightarrow pp\pi^+\pi^-$ reaction we give in section 3 analytic expressions for the non-resonant (Drell-Söding) and the resonant (through the ρ^0 meson) amplitudes. In section 4 we present numerical results for total and differential cross sections and discuss interference effects between the two contributions. Moreover, we will present our prediction for the two-pion invariant mass distribution at LHC energy of 7 TeV in proton-proton collisions, which is currently under analysis by the ALICE and CMS collaborations.

Closely related to the reaction $pp \rightarrow pp\pi^+\pi^-$ studied by us here are the reactions of central $\pi^+\pi^-$ production in ultra-peripheral nucleon-nucleus and nucleus-nucleus collisions, $pA \rightarrow pA\pi^+\pi^-$ and $AA \rightarrow AA\pi^+\pi^-$. For the latter process high-energy data exist from the STAR [31–34] and the ALICE [35] collaborations. For theoretical reviews treating such collisions see for instance [36–38]. The application of our methods, based on the tensor-pomeron concept, to collisions involving nuclei is an interesting problem which, however, goes beyond the scope of the present work.

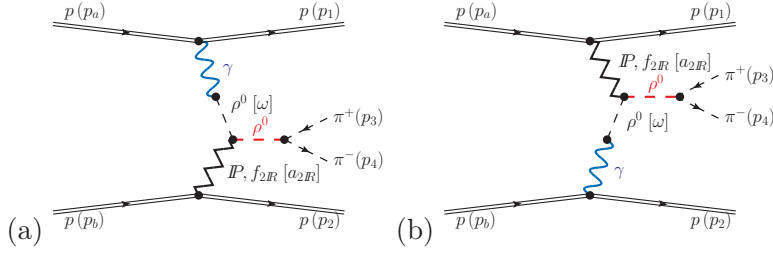


Figure 1. The central exclusive ρ^0 production and its subsequent decay into P -wave $\pi^+\pi^-$ in proton-proton collisions.

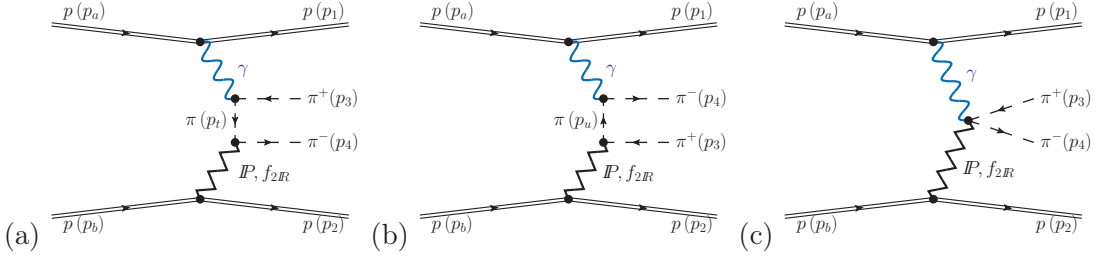


Figure 2. The diagrams for photon-induced central exclusive continuum $\pi^+\pi^-$ production in proton-proton collisions. There are also 3 additional diagrams with the role of $(p(p_a), p(p_1))$ and $(p(p_b), p(p_2))$ exchanged.

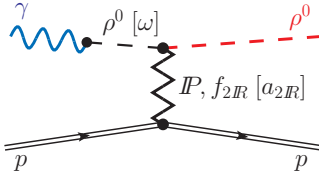


Figure 3. Photoproduction of a ρ^0 meson and its subsequent decay into a $\pi^+\pi^-$ pair via pomeron and subleading reggeon exchanges.

2 Photoproduction of ρ^0 meson

The amplitude for the $\gamma p \rightarrow \rho^0 p$ reaction shown in Fig. 3 includes not only pomeron (P), but also reggeon (f_{2R} , a_{2R}) exchanges.

First, we write down the amplitude for the $\gamma p \rightarrow \rho^0 p$ reaction via the tensor-pomeron exchange as follows

$$\begin{aligned} \langle \rho^0(p_\rho, \lambda_\rho), p(p_2, \lambda_2) | \mathcal{T} | \gamma(q, \lambda_\gamma), p(p_b, \lambda_b) \rangle \equiv \\ \mathcal{M}_{\lambda_\gamma \lambda_b \rightarrow \lambda_\rho \lambda_2} = (-i) (\epsilon^{(\rho)\mu})^* i\Gamma_{\mu\nu\alpha\beta}^{(P\rho\rho)}(p_\rho, q) i\Delta^{(\rho)\nu\kappa}(q) i\Gamma_{\kappa\sigma}^{(\gamma\rightarrow\rho)}(q) \epsilon^{(\gamma)\sigma} \\ \times i\Delta^{(P)\alpha\beta, \delta\eta}(s, t) \bar{u}(p_2, \lambda_2) i\Gamma_{\delta\eta}^{(Ppp)}(p_2, p_b) u(p_b, \lambda_b), \end{aligned} \quad (2.1)$$

where p_b , p_2 and λ_b , $\lambda_2 = \pm\frac{1}{2}$ denote the four-momenta and helicities of the ingoing and outgoing protons, $\epsilon^{(\gamma)}$ and $\epsilon^{(\rho)}$ are the polarisation vectors for photon and ρ^0 meson with the four-momenta q , p_ρ and helicities $\lambda_\gamma = \pm 1$, $\lambda_\rho = \pm 1, 0$, respectively. We use standard

kinematic variables

$$\begin{aligned} s &= W_{\gamma p}^2 = (p_b + q)^2 = (p_2 + p_\rho)^2, \\ t &= (p_2 - p_b)^2 = (p_\rho - q)^2. \end{aligned} \quad (2.2)$$

The $\mathbb{P}\rho\rho$ vertex is given in [16] by formula (3.47). The propagator of the tensor-pomeron exchange is written as (see (3.10) of [16]):

$$i\Delta_{\mu\nu,\kappa\lambda}^{(\mathbb{P})}(s, t) = \frac{1}{4s} \left(g_{\mu\kappa}g_{\nu\lambda} + g_{\mu\lambda}g_{\nu\kappa} - \frac{1}{2}g_{\mu\nu}g_{\kappa\lambda} \right) (-is\alpha'_{\mathbb{P}})^{\alpha_{\mathbb{P}}(t)-1} \quad (2.3)$$

and fulfils the following relations

$$\begin{aligned} \Delta_{\mu\nu,\kappa\lambda}^{(\mathbb{P})}(s, t) &= \Delta_{\nu\mu,\kappa\lambda}^{(\mathbb{P})}(s, t) = \Delta_{\mu\nu,\lambda\kappa}^{(\mathbb{P})}(s, t) = \Delta_{\kappa\lambda,\mu\nu}^{(\mathbb{P})}(s, t), \\ g^{\mu\nu}\Delta_{\mu\nu,\kappa\lambda}^{(\mathbb{P})}(s, t) &= 0, \quad g^{\kappa\lambda}\Delta_{\mu\nu,\kappa\lambda}^{(\mathbb{P})}(s, t) = 0. \end{aligned} \quad (2.4)$$

Here the pomeron trajectory $\alpha_{\mathbb{P}}(t)$ is assumed to be of standard linear form with intercept slightly above 1:

$$\alpha_{\mathbb{P}}(t) = \alpha_{\mathbb{P}}(0) + \alpha'_{\mathbb{P}} t, \quad \alpha_{\mathbb{P}}(0) = 1.0808, \quad \alpha'_{\mathbb{P}} = 0.25 \text{ GeV}^{-2}. \quad (2.5)$$

The corresponding coupling of tensor pomeron to protons (antiprotons) including a vertex form-factor, taken here to be the Dirac electromagnetic form factor of the proton $F_1(t)$ for simplicity (see Section 3.2 of [39]), is written as (see (3.43) of [16]):

$$\begin{aligned} i\Gamma_{\mu\nu}^{(\mathbb{P}pp)}(p', p) &= i\Gamma_{\mu\nu}^{(\mathbb{P}\bar{p}\bar{p})}(p', p) \\ &= -i3\beta_{\mathbb{P}NN}F_1((p' - p)^2) \left\{ \frac{1}{2} [\gamma_\mu(p' + p)_\nu + \gamma_\nu(p' + p)_\mu] - \frac{1}{4}g_{\mu\nu}(\not{p}' + \not{p}) \right\}, \end{aligned} \quad (2.6)$$

where $\not{p} = \gamma_\kappa p^\kappa$ and $\beta_{\mathbb{P}NN} = 1.87 \text{ GeV}^{-1}$. A sufficiently good representation of the Dirac form factor $F_1(t)$ is given by the dipole formula

$$F_1(t) = \frac{4m_p^2 - 2.79 t}{(4m_p^2 - t)(1 - t/m_D^2)^2}, \quad (2.7)$$

where m_p is the proton mass and $m_D^2 = 0.71 \text{ GeV}^2$ is the dipole mass squared.

For the f_{2R} reggeon exchange a similar form of the propagator and the $f_{2R}pp$ effective vertex is assumed, see (3.12) and (3.49) of [16], with the Regge parameters:

$$\alpha_{R_+}(t) = \alpha_{R_+}(0) + \alpha'_{R_+} t, \quad \alpha_{R_+}(0) = 0.5475, \quad \alpha'_{R_+} = 0.9 \text{ GeV}^{-2}. \quad (2.8)$$

The $f_{2R}pp$ vertex is obtained from (2.6) replacing $3\beta_{\mathbb{P}NN}$ by $g_{f_{2R}pp}/M_0$ with $M_0 = 1 \text{ GeV}$ and $g_{f_{2R}pp} = 11.04$.

In the high-energy small-angle approximation we get, using (D.19) in Appendix D of [15],

$$\begin{aligned} \mathcal{M}_{\lambda_\gamma \lambda_b \rightarrow \lambda_\rho \lambda_2}(s, t) &\cong ie \frac{m_\rho^2}{\gamma_\rho} \Delta_T^{(\rho)}(0) (\epsilon^{(\rho)\mu})^* \epsilon^{(\gamma)\nu} V_{\mu\nu\kappa\lambda}(s, t, q, p_\rho) \\ &\quad \times 2(p_2 + p_b)^\kappa (p_2 + p_b)^\lambda \delta_{\lambda_2 \lambda_b} F_1(t) F_M(t). \end{aligned} \quad (2.9)$$

Here $4\pi/\gamma_\rho^2 = 0.496$, $(\Delta_T^{(\rho)}(0))^{-1} = -m_\rho^2$ with the meson mass m_ρ taken from PDG [40]. The function $V_{\mu\nu\kappa\lambda}(s, t, q, p_\rho)$ has the form

$$\begin{aligned} V_{\mu\nu\kappa\lambda}(s, t, q, p_\rho) = & \frac{1}{4s} \\ & \times \left\{ 2\Gamma_{\mu\nu\kappa\lambda}^{(0)}(p_\rho, -q) \left[3\beta_{\mathbb{P}NN} a_{\mathbb{P}\rho\rho} (-is\alpha'_{\mathbb{P}})^{\alpha_{\mathbb{P}}(t)-1} + M_0^{-1} g_{f_2\mathbb{R}pp} a_{f_2\mathbb{R}\rho\rho} (-is\alpha'_{\mathbb{R}+})^{\alpha_{\mathbb{R}+}(t)-1} \right] \right. \\ & \left. - \Gamma_{\mu\nu\kappa\lambda}^{(2)}(p_\rho, -q) \left[3\beta_{\mathbb{P}NN} b_{\mathbb{P}\rho\rho} (-is\alpha'_{\mathbb{P}})^{\alpha_{\mathbb{P}}(t)-1} + M_0^{-1} g_{f_2\mathbb{R}pp} b_{f_2\mathbb{R}\rho\rho} (-is\alpha'_{\mathbb{R}+})^{\alpha_{\mathbb{R}+}(t)-1} \right] \right\}, \end{aligned} \quad (2.10)$$

where the explicit tensorial functions $\Gamma_{\mu\nu\kappa\lambda}^{(i)}(p_\rho, -q)$, $i = 0, 2$, are given in Ref. [16], formulae (3.18) and (3.19), respectively. In (2.9) $F_M(t)$ is the pion electromagnetic form factor in a parametrization valid for $t < 0$,

$$F_M(t) = \frac{1}{1 - t/\Lambda_0^2}, \quad (2.11)$$

where $\Lambda_0^2 = 0.5 \text{ GeV}^2$; see e.g. (3.22) of [39] and (3.34) of [16].

Fig. 4 (left panel) shows the integrated cross section for the $\gamma p \rightarrow \rho^0 p$ reaction, calculated from (2.9), as function of the center-of-mass energy together with the experimental data. We have checked that the cross section from the $a_{2\mathbb{R}}$ -exchange is about three orders of magnitude smaller than from the $f_{2\mathbb{R}}$ -exchange. This is due to the fact, that the γ - ω coupling is much smaller than the γ - ρ coupling and $g_{a_{2\mathbb{R}pp}} \ll g_{f_{2\mathbb{R}pp}}$; see (3.50) and (3.52) of [16]. Thus, in the present calculations we have neglected the $a_{2\mathbb{R}}$ -exchange contribution. As shown in [16] the $\mathbb{P}\rho\rho$ and $f_{2\mathbb{R}\rho\rho}$ coupling constants a and b are expected to approximately fulfil the relations: ¹

$$2m_\rho^2 a_{\mathbb{P}\rho\rho} + b_{\mathbb{P}\rho\rho} = 4\beta_{\mathbb{P}\pi\pi} = 7.04 \text{ GeV}^{-1}, \quad (2.12)$$

$$2m_\rho^2 a_{f_{2\mathbb{R}\rho\rho}} + b_{f_{2\mathbb{R}\rho\rho}} = M_0^{-1} g_{f_{2\mathbb{R}\pi\pi}} = 9.30 \text{ GeV}^{-1}; \quad (2.13)$$

see (7.27) and (7.28) of [16]. In our calculations two parameter sets of coupling constants are used:

$$\begin{aligned} \text{set A : } & a_{\mathbb{P}\rho\rho} = 0.7 \text{ GeV}^{-3}, a_{f_{2\mathbb{R}\rho\rho}} = 0 \text{ GeV}^{-3}, \\ & b_{\mathbb{P}\rho\rho} = 6.2 \text{ GeV}^{-1}, b_{f_{2\mathbb{R}\rho\rho}} = 9.3 \text{ GeV}^{-1}, \end{aligned} \quad (2.14)$$

$$\text{set B : } a_{\mathbb{P}\rho\rho} = a_{f_{2\mathbb{R}\rho\rho}} = 0 \text{ GeV}^{-3}, b_{\mathbb{P}\rho\rho} = 7.04 \text{ GeV}^{-1}, b_{f_{2\mathbb{R}\rho\rho}} = 9.3 \text{ GeV}^{-1}. \quad (2.15)$$

At low energies there are other processes contributing, such as meson exchanges (e.g. π^0 , η , σ), the ρ^0 bremsstrahlung, baryonic resonances decaying into the $\rho^0 p$ channel etc. Thus, the Regge terms should not be expected to fit the low-energy data precisely. We refer the reader to [41–46] for reviews and details concerning the ρ^0 photoproduction mechanism at

¹The coupling constants of the leading trajectories in Eq. (2.10) have been estimated from the parametrization of total cross sections for $\pi^+ p$ and $\pi^- p$ scattering assuming $\sigma_{tot}(\rho^0(\epsilon^{(\lambda\rho)}), p) = \frac{1}{2} [\sigma_{tot}(\pi^+, p) + \sigma_{tot}(\pi^-, p)]$ for $\lambda_\rho = \pm 1$. The theoretical formulae of total πp cross sections are discussed in Section 7.1 of [16].

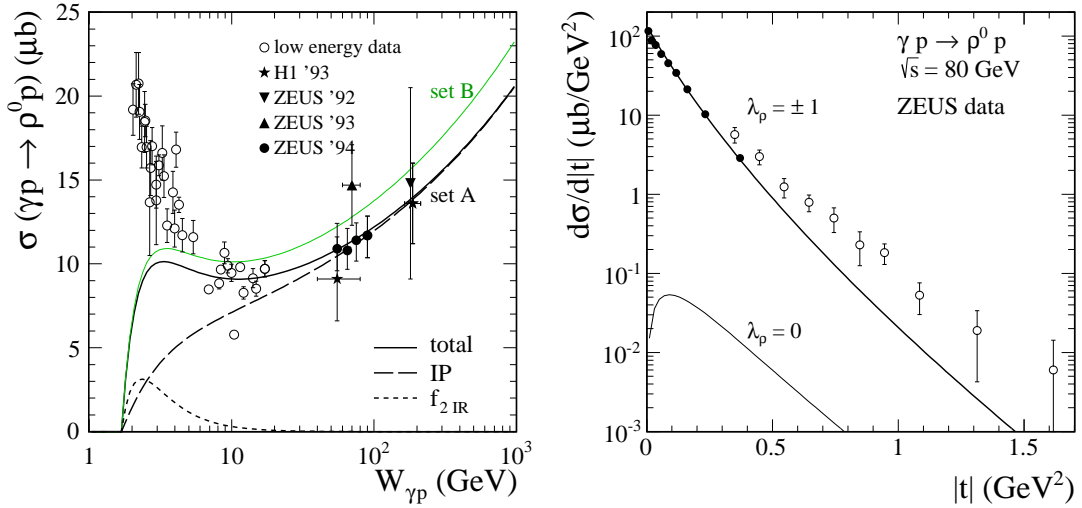


Figure 4. Left panel: The elastic ρ^0 photoproduction cross section as a function of the center-of-mass energy $W_{\gamma p}$. Our results are compared with the HERA data [47, 49–52] (solid marks) and with a compilation of low energy data (open circles); see Fig. 10 of Ref. [47] for more references. The solid line corresponds to results with both the pomeron and f_{2R} exchanges. The individual pomeron and reggeon exchange contributions denoted by the long-dashed and short-dashed lines, respectively, are presented. The black lines represent parameter set A of coupling constants given by (2.14) while the green line represents set B (2.15). Right panel: The differential cross section $d\sigma/d|t|$ for the $\gamma p \rightarrow \rho^0 p$ process. The ZEUS data at low $|t|$ (at γp average center-of-mass energy $<\sqrt{s}> = 71.7$ GeV [47]) and at higher $|t|$ (at $<\sqrt{s}> = 94$ GeV [48]) are shown. The top and bottom lines represent the results at $\sqrt{s} = 80$ GeV for ρ^0 meson transverse ($\lambda_\rho = \pm 1$) and longitudinal ($\lambda_\rho = 0$) polarisation, respectively. Here we have used parameter set A of coupling constants given by (2.14).

low energies. We see from Fig. 4, left panel, that our model calculation describes the total cross section for $\gamma p \rightarrow \rho^0 p$ fairly well for energies $W_{\gamma p} \gtrsim 8$ GeV.

In the right panel of Fig. 4 we show the differential cross section for elastic ρ^0 photoproduction. The calculations, performed for $\sqrt{s} = 80$ GeV, are compared with ZEUS data [47, 48]. We can see that, according to our calculation, the amplitude for longitudinal ρ^0 meson polarisation is negligible and vanishes at $t = 0$. The sum of the $\lambda_\rho = \pm 1$ contributions describes the data well up to $|t| \approx 0.5$ GeV².

In Ref. [17] detailed model calculations for the reaction $\gamma p \rightarrow \pi^+ \pi^- p$ have been presented using the approach to soft scattering from [16]. The diagrams considered in [17] include ρ^0 production, as in our Fig. 3, but also a number of other processes; see Fig. 1 of [17]. Our results here for ρ^0 production are in agreement with those from [17]; see Figs. 3 and 4 there. This gives a very valuable cross check of the programs used for the calculations in [17] and in our present paper. We shall now go on and calculate with the same methods amplitudes and cross sections corresponding to the diagrams of Figs. 1 and 2.

3 The central exclusive two-pion production

We shall study exclusive production of $\pi^+\pi^-$ in proton-proton collisions at high energies

$$p(p_a, \lambda_a) + p(p_b, \lambda_b) \rightarrow p(p_1, \lambda_1) + \pi^+(p_3) + \pi^-(p_4) + p(p_2, \lambda_2), \quad (3.1)$$

where $p_{a,b}$, $p_{1,2}$ and $\lambda_{a,b}$, $\lambda_{1,2} = \pm\frac{1}{2}$ denote the four-momenta and helicities of the protons, and $p_{3,4}$ denote the four-momenta of the charged pions, respectively. In the following we will calculate the contributions from the diagrams of Figs. 1 and 2 to the process (3.1), that is, the photon-pomeron and photon- f_{2R} reggeon exchange contributions. These processes are expected to be the dominant ones for highly peripheral pp -collisions. Experimentally such collision could be selected by requiring only a very small deflection angle for at least one of the outgoing protons.

The kinematic variables for reaction (3.1) are

$$\begin{aligned} p_{34} &= p_3 + p_4, \quad q_1 = p_a - p_1, \quad q_2 = p_b - p_2, \\ s &= (p_a + p_b)^2 = (p_1 + p_2 + p_{34})^2, \quad M_{\pi\pi}^2 = p_{34}^2, \\ s_1 &= (p_a + q_2)^2 = (p_1 + p_{34})^2, \quad s_2 = (p_b + q_1)^2 = (p_2 + p_{34})^2, \\ t_1 &= q_1^2, \quad t_2 = q_2^2; \end{aligned} \quad (3.2)$$

see also Appendix D of [15].

The Born amplitude for exclusive photoproduction of $\pi^+\pi^-$ can be written as the following sum:

$$\mathcal{M}_{pp \rightarrow pp\pi^+\pi^-}^{Born} = \mathcal{M}^{(\gamma P)} + \mathcal{M}^{(P\gamma)} + \mathcal{M}^{(\gamma f_{2R})} + \mathcal{M}^{(f_{2R}\gamma)}. \quad (3.3)$$

If we want to treat $p\bar{p}$ -collisions (Tevatron) we must be careful since then there is no symmetry any more for the amplitude under $p(p_a) \leftrightarrow p(p_b)$, $p(p_1) \leftrightarrow p(p_2)$, etc. Using the charge conjugation (C) properties of the γ , P and f_{2R} exchanges we get for $p\bar{p}$ scattering from (3.3)

$$\mathcal{M}_{p\bar{p} \rightarrow p\bar{p}\pi^+\pi^-}^{Born} = \mathcal{M}^{(\gamma P)} - \mathcal{M}^{(P\gamma)} + \mathcal{M}^{(\gamma f_{2R})} - \mathcal{M}^{(f_{2R}\gamma)}. \quad (3.4)$$

Note that these sign changes are automatically obtained using the Feynman rules for the tensor pomeron and f_{2R} exchanges but have to be implemented by hand for the vectorial pomeron and f_{2R} exchanges.

3.1 ρ^0 -resonance contribution

The “bare” amplitude (excluding rescattering effects) for the γP -exchange, see diagram (a) in Fig. 1, can be written in terms of our building blocks as follows:

$$\begin{aligned} \mathcal{M}_{\lambda_a \lambda_b \rightarrow \lambda_1 \lambda_2 \pi^+ \pi^-}^{(\gamma P)} &= (-i) \bar{u}(p_1, \lambda_1) i\Gamma_\mu^{(\gamma pp)}(p_1, p_a) u(p_a, \lambda_a) \\ &\times i\Delta^{(\gamma) \mu\sigma}(q_1) i\Gamma_{\sigma\nu}^{(\gamma \rightarrow \rho)}(q_1) i\Delta^{(\rho) \nu\rho_1}(q_1) i\Delta^{(\rho) \rho_2\kappa}(p_{34}) i\Gamma_\kappa^{(\rho\pi\pi)}(p_3, p_4) \\ &\times i\Gamma_{\rho_2\rho_1\alpha\beta}^{(P\rho\rho)}(p_{34}, q_1) i\Delta^{(P) \alpha\beta, \delta\eta}(s_2, t_2) \bar{u}(p_2, \lambda_2) i\Gamma_{\delta\eta}^{(Ppp)}(p_2, p_b) u(p_b, \lambda_b). \end{aligned} \quad (3.5)$$

All propagators and vertices used in (3.5) are defined in section 3 of [16]; see also Appendix B of [17]. For the $\mathbb{P}\gamma$ -exchange the amplitude has the same structure with $p(p_a), p(p_1) \leftrightarrow p(p_b), p(p_2)$, $t_1 \leftrightarrow t_2$ and $s_2 \leftrightarrow s_1$. In a similar way we can write down the γf_{2R} and $f_{2R}\gamma$ amplitudes.

For simplicity, in the following we shall consider the amplitude (3.5) in the high-energy small-angle limit; see Appendix D of [15]. Including both, pomeron and f_{2R} exchanges, we obtain in this way

$$\begin{aligned} \mathcal{M}_{\lambda_a \lambda_b \rightarrow \lambda_1 \lambda_2 \pi^+ \pi^-}^{(\gamma \mathbb{P} + \gamma f_{2R})} &\simeq ie(p_1 + p_a)^\mu F_1(t_1) \delta_{\lambda_1 \lambda_a} \\ &\times e \frac{m_\rho^2}{\gamma_\rho} \frac{1}{t_1} \Delta_{\mu\rho_1}^{(\rho)}(q_1) \Delta_{\rho_2\kappa}^{(\rho)}(p_{34}) \frac{g_{\rho\pi\pi}}{2} (p_3 - p_4)^\kappa \tilde{F}^{(\rho)}(q_1^2) \tilde{F}^{(\rho)}(p_{34}^2) \\ &\times V^{\rho_2\rho_1\alpha\beta}(s_2, t_2, q_1, p_{34}) F_M(t_2) 2(p_2 + p_b)_\alpha (p_2 + p_b)_\beta F_1(t_2) \delta_{\lambda_2 \lambda_b}. \end{aligned} \quad (3.6)$$

The function $V^{\rho_2\rho_1\alpha\beta}(s_2, t_2, q_1, p_{34})$ is as defined in (2.10) and includes two tensorial functions $\Gamma^{(i)\rho_2\rho_1\alpha\beta}(p_{34}, -q_1)$ for $i = 0, 2$. From (3.21) and (3.22) of [16] we have

$$\begin{aligned} q_1^{\rho_1} \Gamma_{\rho_2\rho_1\alpha\beta}^{(i)}(p_{34}, -q_1) &= 0, \quad p_{34}^{\rho_2} \Gamma_{\rho_2\rho_1\alpha\beta}^{(i)}(p_{34}, -q_1) = 0, \\ g^{\alpha\beta} \Gamma_{\rho_2\rho_1\alpha\beta}^{(i)}(p_{34}, -q_1) &= 0, \quad i = 0, 2. \end{aligned} \quad (3.7)$$

Thus, the terms proportional to $q_1^\mu q_1^{\rho_1}$ in $\Delta^{(\rho)\mu\rho_1}(q_1)$ cannot contribute. The same is true for the terms proportional to $p_{34}^{\rho_2} p_{34}^\kappa$ in $\Delta^{(\rho)\rho_2\kappa}(p_{34})$. Thus, only the transverse part of the ρ^0 propagator $\Delta_T^{(\rho)}(k^2)$, as defined in (4.1)-(4.4) of [16], contributes in (3.6). As is easily seen, the same holds for (3.5). The decay vertex for $\rho^0 \rightarrow \pi^+\pi^-$ is well known (e.g. see (3.35) of [16]) and the relevant coupling constant is $g_{\rho\pi\pi} = 11.51$. We emphasize that in the work [53] the authors found a very good description of the ρ line shape from the $e^+e^- \rightarrow \pi^+\pi^-$ reaction - up to $k^2 \cong 2 \text{ GeV}^2$ - without a form factor in the $\rho\pi\pi$ vertex.

In the diagram of Fig. 1 at the pomeron- ρ - ρ vertex the incoming ρ is always off shell, the outgoing ρ also may be away from the nominal “mass shell” $p_{34}^2 = m_\rho^2$. As suggested in [17], see (B.82) there, we insert, therefore, in the $\mathbb{P}\rho\rho$ vertex extra form factors. A convenient form, given in (B.85) of [17] is

$$\tilde{F}^{(\rho)}(k^2) = \left[1 + \frac{k^2(k^2 - m_\rho^2)}{\Lambda_\rho^4} \right]^{-n_\rho}. \quad (3.8)$$

The form factor (3.8) has the property: $\tilde{F}^{(\rho)}(0) = \tilde{F}^{(\rho)}(m_\rho^2) = 1$ which is consistent with the traditional, phenomenologically successful, vector-meson-dominance model.

3.2 Drell-Söding contribution

The γP -exchange amplitudes given by the diagrams shown in Fig. 2, can be written on the Born level for the tensor-pomeron exchange as follows

$$\begin{aligned} \mathcal{M}_{\lambda_a \lambda_b \rightarrow \lambda_1 \lambda_2 \pi^+ \pi^-}^{(a)} &= (-i) \bar{u}(p_1, \lambda_1) i \Gamma_{\mu}^{(\gamma pp)}(p_1, p_a) u(p_a, \lambda_a) i \Delta^{(\gamma) \mu \nu}(q_1) i \Gamma_{\nu}^{(\gamma \pi \pi)}(p_t, -p_3) \\ &\quad \times i \Delta^{(\pi)}(p_t) i \Gamma_{\alpha \beta}^{(P \pi \pi)}(p_4, p_t) i \Delta^{(P) \alpha \beta, \delta \eta}(s_2, t_2) \bar{u}(p_2, \lambda_2) i \Gamma_{\delta \eta}^{(P pp)}(p_2, p_b) u(p_b, \lambda_b), \end{aligned} \quad (3.9)$$

$$\begin{aligned} \mathcal{M}_{\lambda_a \lambda_b \rightarrow \lambda_1 \lambda_2 \pi^+ \pi^-}^{(b)} &= (-i) \bar{u}(p_1, \lambda_1) i \Gamma_{\mu}^{(\gamma pp)}(p_1, p_a) u(p_a, \lambda_a) i \Delta^{(\gamma) \mu \nu}(q_1) i \Gamma_{\nu}^{(\gamma \pi \pi)}(p_4, p_u) \\ &\quad \times i \Delta^{(\pi)}(p_u) i \Gamma_{\alpha \beta}^{(P \pi \pi)}(p_u, -p_3) i \Delta^{(P) \alpha \beta, \delta \eta}(s_2, t_2) \bar{u}(p_2, \lambda_2) i \Gamma_{\delta \eta}^{(P pp)}(p_2, p_b) u(p_b, \lambda_b), \end{aligned} \quad (3.10)$$

$$\begin{aligned} \mathcal{M}_{\lambda_a \lambda_b \rightarrow \lambda_1 \lambda_2 \pi^+ \pi^-}^{(c)} &= (-i) \bar{u}(p_1, \lambda_1) i \Gamma_{\mu}^{(\gamma pp)}(p_1, p_a) u(p_a, \lambda_a) i \Delta^{(\gamma) \mu \nu}(q_1) \\ &\quad \times i \Gamma_{\nu, \alpha \beta}^{(P \gamma \pi \pi)}(q_1, p_4, -p_3) i \Delta^{(P) \alpha \beta, \delta \eta}(s_2, t_2) \bar{u}(p_2, \lambda_2) i \Gamma_{\delta \eta}^{(P pp)}(p_2, p_b) u(p_b, \lambda_b). \end{aligned} \quad (3.11)$$

Above we have introduced $p_t = p_a - p_1 - p_3$ and $p_u = p_4 - p_a + p_1$. In order to assure gauge invariance and “proper” cancellations among the three terms (3.9) to (3.11) we have introduced, somewhat arbitrarily, one common energy dependence s_2 for the pomeron propagator in all three diagrams instead of naively s_{24} , s_{23} , and s_2 , respectively, where $s_{ij} = (p_i + p_j)^2$. See also the discussion of this point in section 2.5 of [17] where a justification for this procedure is given.

For the $P\gamma$ -exchange we have the same structure as for the above amplitudes with $p(p_a), p(p_1) \leftrightarrow p(p_b), p(p_2)$, $t_2 \leftrightarrow t_1$, $s_2 \leftrightarrow s_1$. In a similar way we can write the γf_{2R} and $f_{2R}\gamma$ amplitudes.

Starting with the $P\pi\pi$ coupling, see Eq. (7.3) of [16], and making a minimal substitution there gives the couplings involving pions, photons and the pomeron (see (B.66) to (B.71) of [17]). We have the following vertex, see Eq.(3.45) of [16] and (B.69) of [17],

$$i \Gamma_{\alpha \beta}^{(P \pi \pi)}(k', k) = -i 2 \beta_{P \pi \pi} \left[(k' + k)_{\alpha} (k' + k)_{\beta} - \frac{1}{4} g_{\alpha \beta} (k' + k)^2 \right] F_M((k' - k)^2), \quad (3.12)$$

where $\beta_{P \pi \pi} = 1.76 \text{ GeV}^{-1}$. For the standard electromagnetic vertex we have

$$i \Gamma_{\nu}^{(\gamma \pi \pi)}(k', k) = i e (k' + k)_{\nu} F_M((k' - k)^2). \quad (3.13)$$

Finally, there is the contact term, see (B.71) of [17],

$$\begin{aligned} i \Gamma_{\nu, \alpha \beta}^{(P \gamma \pi \pi)}(q, k', k) &= -i e 2 \beta_{P \pi \pi} [2 g_{\alpha \nu} (k' + k)_{\beta} + 2 g_{\beta \nu} (k' + k)_{\alpha} - g_{\alpha \beta} (k' + k)_{\nu}] \\ &\quad \times F_M(q^2) F_M((k' - q - k)^2). \end{aligned} \quad (3.14)$$

Compared to (B.67) and (B.71) of [17] we have introduced in both, (3.13) and (3.14), an extra form factor $F_M(q^2)$ (2.11). For an on shell photon with $q^2 = 0$ this form factor is equal to 1 and, thus, would not make any difference for the calculations of photoproduction in [17]. With the normal pion propagator $i \Delta^{(\pi)}(k) = i/(k^2 - m_{\pi}^2)$ the above ansatz for the vertices guarantees gauge invariance of the $\pi^+ \pi^-$ continuum contribution.

In the high-energy approximation we can write for tensor-pomeron exchange

$$\begin{aligned}\mathcal{M}_{\lambda_a \lambda_b \rightarrow \lambda_1 \lambda_2 \pi^+ \pi^-}^{(a)} &\simeq ie^2 (p_1 + p_a)^\mu \delta_{\lambda_1 \lambda_a} F_1(t_1) F_M(t_1) \frac{1}{t_1} (p_t - p_3)_\mu \frac{1}{p_t^2 - m_\pi^2} \\ &\times 2\beta_{\mathbb{P}\pi\pi} (p_4 + p_t)^\alpha (p_4 + p_t)^\beta \frac{1}{4s_2} (-is_2 \alpha'_{\mathbb{P}})^{\alpha_{\mathbb{P}}(t_2)-1} \\ &\times 3\beta_{\mathbb{P}NN} 2(p_2 + p_b)_\alpha (p_2 + p_b)_\beta \delta_{\lambda_2 \lambda_b} F_1(t_2) F_M(t_2),\end{aligned}\quad (3.15)$$

$$\begin{aligned}\mathcal{M}_{\lambda_a \lambda_b \rightarrow \lambda_1 \lambda_2 \pi^+ \pi^-}^{(b)} &\simeq ie^2 (p_1 + p_a)^\mu \delta_{\lambda_1 \lambda_a} F_1(t_1) F_M(t_1) \frac{1}{t_1} (p_4 + p_u)_\mu \frac{1}{p_u^2 - m_\pi^2} \\ &\times 2\beta_{\mathbb{P}\pi\pi} (p_u - p_3)^\alpha (p_u - p_3)^\beta \frac{1}{4s_2} (-is_2 \alpha'_{\mathbb{P}})^{\alpha_{\mathbb{P}}(t_2)-1} \\ &\times 3\beta_{\mathbb{P}NN} 2(p_2 + p_b)_\alpha (p_2 + p_b)_\beta \delta_{\lambda_2 \lambda_b} F_1(t_2) F_M(t_2),\end{aligned}\quad (3.16)$$

$$\begin{aligned}\mathcal{M}_{\lambda_a \lambda_b \rightarrow \lambda_1 \lambda_2 \pi^+ \pi^-}^{(c)} &\simeq -ie^2 (p_1 + p_a)^\nu \delta_{\lambda_1 \lambda_a} \frac{1}{t_1} F_1(t_1) F_M(t_1) \\ &\times 2\beta_{\mathbb{P}\pi\pi} [2g_{\alpha\nu} (p_4 - p_3)_\beta + 2g_{\beta\nu} (p_4 - p_3)_\alpha] \frac{1}{4s_2} (-is_2 \alpha'_{\mathbb{P}})^{\alpha_{\mathbb{P}}(t_2)-1} \\ &\times 3\beta_{\mathbb{P}NN} 2(p_2 + p_b)^\alpha (p_2 + p_b)^\beta \delta_{\lambda_2 \lambda_b} F_1(t_2) F_M(t_2).\end{aligned}\quad (3.17)$$

Gauge invariance of our expressions can be checked explicitly. As it should be we find from (3.15) to (3.17)

$$\{\mathcal{M}^{(a)} + \mathcal{M}^{(b)} + \mathcal{M}^{(c)}\}|_{p_1+p_a \rightarrow q_1} = 0. \quad (3.18)$$

For the $f_{2\mathbb{R}}$ -reggeon exchange the formulae have the same tensorial structure and are obtained from (3.15) to (3.17) with the replacements discussed in the paragraph including (2.8). The formulae above do not include hadronic form factors for the inner subprocesses $\gamma \mathbb{P} \rightarrow \pi\pi$.

A possible way to include form factors for the inner subprocesses is to multiply the amplitude obtained from (3.15) to (3.17) with a common factor, see [54–56],

$$\mathcal{M}^{(\gamma \mathbb{P})} = (\mathcal{M}^{(a)} + \mathcal{M}^{(b)} + \mathcal{M}^{(c)}) F(p_t^2, p_u^2, p_{34}^2). \quad (3.19)$$

A common form factor for all three diagrams is chosen in order to maintain gauge invariance, and a convenient form is

$$F(p_t^2, p_u^2, p_{34}^2) = \frac{F^2(p_t^2) + F^2(p_u^2)}{1 + F^2(-p_{34}^2)}. \quad (3.20)$$

Here we take the monopole form factor which is normalized to unity at the on-shell point $F(m_\pi^2) = 1$:

$$F(p^2) = \frac{\Lambda_\pi^2 - m_\pi^2}{\Lambda_\pi^2 - p^2}. \quad (3.21)$$

with Λ_π being a free parameter. We expect it in the range of 0.8 to 1 GeV.

3.3 Absorptive corrections

We should add the absorptive corrections to the Born amplitude (3.3) to give the full physical amplitude for the $pp \rightarrow pp\pi^+\pi^-$ reaction, i.e. we have

$$\mathcal{M}_{pp \rightarrow pp\pi^+\pi^-} = \mathcal{M}_{pp \rightarrow pp\pi^+\pi^-}^{\text{Born}} + \mathcal{M}_{pp \rightarrow pp\pi^+\pi^-}^{\text{pp-rescattering}}. \quad (3.22)$$

Here (and above) we have for simplicity omitted the dependence of the amplitude on kinematic variables. The details how to conveniently reduce the number of kinematic integration variables are discussed in [11].

The amplitude including pp -rescattering corrections in the four-body reaction discussed here is given by ²

$$\mathcal{M}_{pp \rightarrow pp\pi^+\pi^-}^{\text{pp-rescattering}}(s, \mathbf{p}_{1\perp}, \mathbf{p}_{2\perp}) = \frac{i}{8\pi^2 s} \int d^2 \mathbf{k}_{\perp} \mathcal{M}_{pp \rightarrow pp}(s, -\mathbf{k}_{\perp}^2) \mathcal{M}_{pp \rightarrow pp\pi^+\pi^-}^{\text{Born}}(s, \tilde{\mathbf{p}}_{1\perp}, \tilde{\mathbf{p}}_{2\perp}), \quad (3.23)$$

where $\tilde{\mathbf{p}}_{1\perp} = \mathbf{p}_{1\perp} - \mathbf{k}_{\perp}$ and $\tilde{\mathbf{p}}_{2\perp} = \mathbf{p}_{2\perp} + \mathbf{k}_{\perp}$. Here, in the overall c.m. system, $\mathbf{p}_{1\perp}$ and $\mathbf{p}_{2\perp}$ are the transverse components of the momenta of the final-state protons and \mathbf{k}_{\perp} is the transverse momentum carried around the pomeron loop. $\mathcal{M}_{pp \rightarrow pp}(s, -\mathbf{k}_{\perp}^2)$ is the elastic pp scattering amplitude given by Eq. (6.28) in [16] for large s and with the momentum transfer $t = -\mathbf{k}_{\perp}^2$.

4 Results

In this section we present some selected results for cross sections for the discussed photoproduction processes. In calculating the cross section of the four-body process (3.1) we perform integrations in auxiliary variables $\xi_1 = \log_{10}(p_{1\perp}/1 \text{ GeV})$ and $\xi_2 = \log_{10}(p_{2\perp}/1 \text{ GeV})$ instead of the outgoing proton's transverse momenta ($p_{1\perp}$ and $p_{2\perp}$). For example $\xi_1 = -1$ means $p_{1\perp} = 0.1 \text{ GeV}$. The correlation between the variables ξ_1 and ξ_2 is displayed in Fig. 5 at center-of-mass energy at $\sqrt{s} = 7 \text{ TeV}$. Here we include both the resonant and non-resonant contributions. The projection on one of the axes is shown in Fig. 6 at two incident energies at $\sqrt{s} = 0.5$ and 7 TeV . The parameters of the model used here are indicated in the legend of Fig. 5.

In Fig. 7 we show the two-pion invariant mass distributions for the Drell-Söding contribution alone at two c.m. energies $\sqrt{s} = 0.5$ and 7 TeV , see the lower and upper lines, respectively. The solid lines correspond to the tensor pomeron and f_{2R} exchanges in the amplitude while the dashed lines correspond to the pomeron exchange alone. At the lower energy one can observe a larger interference effect between the $\gamma \mathbb{P}$ ($\mathbb{P} \gamma$) and the γf_{2R} ($f_{2R} \gamma$) components in the amplitude (3.3).

Now we turn to the full calculation including the resonant and the non-resonant (Drell-Söding) contributions. These have to be added at the amplitude level and then squared to get the cross sections including all interference effects. In Fig. 8 we show the resulting

²We refer the reader to [25–29] for reviews of three-body processes and details concerning the absorption corrections in the eikonal approximation which takes into account the contribution of elastic pp -rescattering.

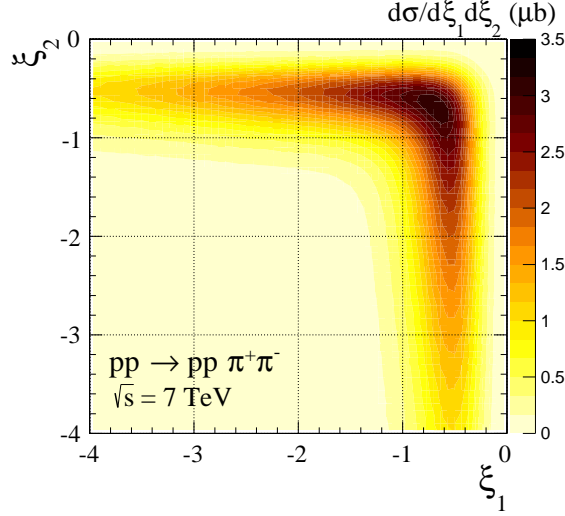


Figure 5. Two-dimensional distribution in the auxiliary variables $\xi_1 = \log_{10}(p_{1\perp}/1 \text{ GeV})$ and $\xi_2 = \log_{10}(p_{2\perp}/1 \text{ GeV})$ for the photoproduction mechanism at $\sqrt{s} = 7 \text{ TeV}$. Plotted is $d\sigma/d\xi_1 d\xi_2$ in μb . In the calculation we have used the parameter set A of coupling constants given by (2.14) and we have taken $\Lambda_\rho = 2 \text{ GeV}$ and $n_\rho = 0.5$ in (3.8).

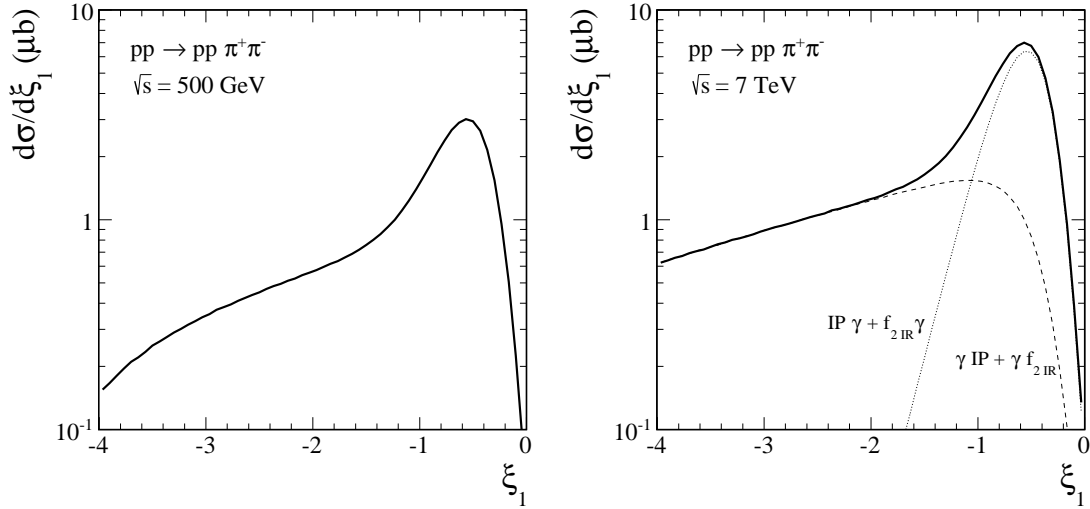


Figure 6. The distributions in ξ_1 at two incident energies $\sqrt{s} = 0.5$ and 7 TeV . The solid line corresponds to the situation when all, that is, the pomeron and f_{2R} exchanges in the amplitude are included. The short-dashed and dotted lines represent the contributions from $\gamma - \mathbb{P}/\mathbb{R}$ and $\mathbb{P}/\mathbb{R} - \gamma$ exchanges, respectively.

two-pion invariant-mass distribution for two different scenarios. In the first scenario (left panel) we take a relatively hard form factor for the resonant contribution and no form factors for the inner process for the non-resonant contribution. In our calculations we set $\Lambda_\rho = 2 \text{ GeV}$ and $n_\rho = 0.4, 0.5$, or 0.6 in (3.8) and $F(p_t^2, p_u^2, p_{34}^2) = 1$ in (3.20). This is the scenario discussed recently in [17]. In this scenario strong interference effects can be

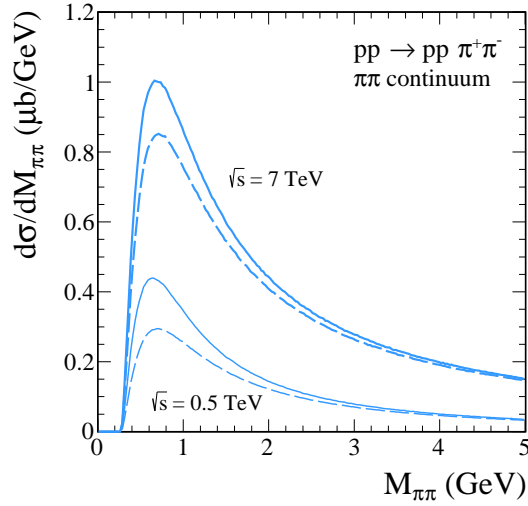


Figure 7. Two-pion continuum (Drell-Söding) contributions at $\sqrt{s} = 0.5$ TeV (lower lines) and 7 TeV (upper lines). The solid lines correspond to the tensor pomeron and $f_{2\mathbb{R}}$ exchanges in the amplitudes while the dashed lines correspond to the pomeron exchange alone. No extra form factors (3.20) for inner subprocesses are included.

observed. These effects strongly depend on the details of the form factor (compare the three different lines, corresponding to the three different values of n_ρ , in the left panel of Fig. 8). In the present paper we consider also a second scenario (right panel) with softer form factor (3.8) ($\Lambda_\rho = 1$ GeV, $n_\rho = 0.6$ and 0.7) and including monopole-like form factors (3.20), (3.21), for the inner processes with $\Lambda_\pi = 0.8$ GeV. The final result for the two scenarios is rather similar. Therefore, in the following presentation we shall use only the first scenario as representative.

In Fig. 9 we show the interference effect in the ρ^0 mass region. The skewing of the ρ^0 shape caused by the interference of the resonant and non-resonant contributions is clearly exposed. The skewing depends crucially on the choice of the ρ^0 form factor parameterisation (3.8).

In Fig. 10 we present distributions in pion transverse momentum $p_{\perp,\pi}$, i.e. p_{\perp,π^+} or p_{\perp,π^-} . At small $p_{\perp,\pi}$ the resonance contribution is the dominant one. At higher $p_{\perp,\pi}$ our calculation, with the chosen model parameters, gives a strong cancellation between the resonant and the non-resonant terms.

In Fig. 11 we show rapidity y_π and pseudorapidity η_π distributions of pions produced in the photoproduction mechanism. The $f_{2\mathbb{R}}$ exchange included in the amplitude contributes mainly at backward and forward pion rapidities. Its contribution is nonnegligible even at the LHC. The dip in the η_π distribution for $|\eta_\pi| \rightarrow 0$ is a kinematic effect; see Appendix D of [15].

The correlation between y_{π^+} and y_{π^-} is displayed in Fig. 12. One can observe a strong correlation between y_{π^+} and y_{π^-} . This correlation is similar to the correlation studied in [11, 12] for the Regge-like diffractive production of $\pi^+\pi^-$ continuum, i.e. the pions are emitted preferentially in the same hemispheres. In contrast to the \mathbb{P}/\mathbb{R} - \mathbb{P}/\mathbb{R} fusion [11],

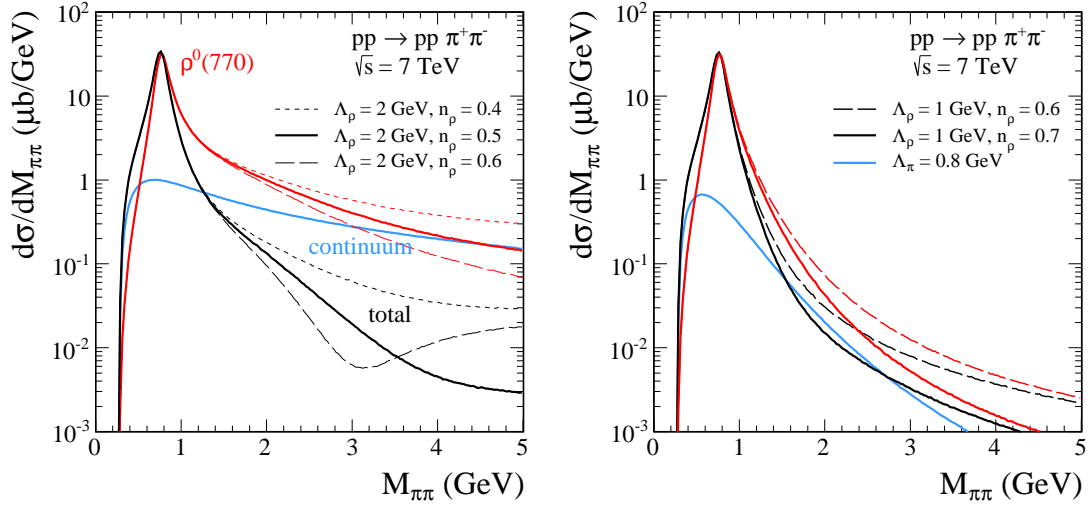


Figure 8. Two-pion invariant mass distributions at $\sqrt{s} = 7$ TeV for two different scenarios discussed in the main text. The ρ^0 (red lines), continuum (blue lines) and total (black lines) contributions are shown. The left panel corresponds to a “hard” form factor (3.8) and the form factor $F(p_t^2, p_u^2, p_{34}^2) = 1$ in (3.20) for the inner processes. The right panel corresponds to a “soft” form factor (3.8) and a non-trivial form factor (3.21) for the inner processes.

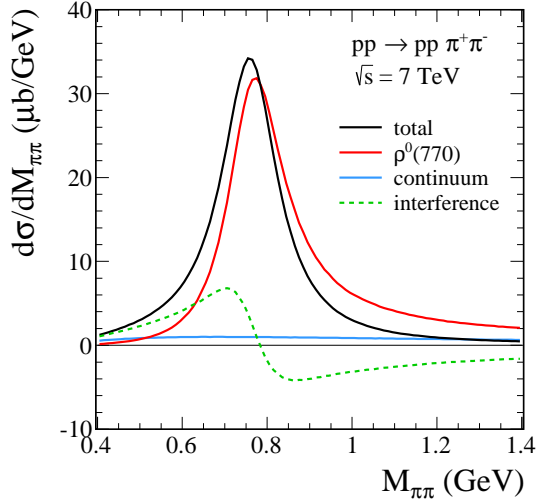


Figure 9. Two-pion invariant mass distribution at $\sqrt{s} = 7$ TeV for the resonant and non-resonant contributions as well as their coherent sum. The interference term of ρ^0 with the $\pi^+\pi^-$ continuum is also shown. We have taken here $\Lambda_\rho = 2$ GeV and $n_\rho = 0.5$ in (3.8).

where the camel-like shape was predicted, no large $|y_\pi|$ enhancement is predicted for the photoproduction case.

In Fig. 13 we show the cross section as a function of the azimuthal angle between the transverse momentum vectors of the two outgoing protons (left panel) and between the outgoing pions (right panel) for the photoproduction mechanism. In the first case the

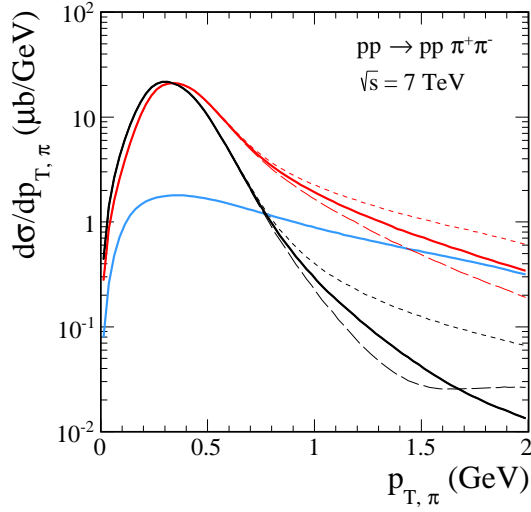


Figure 10. The distributions in pion transverse momentum for the central exclusive $\rho^0 \rightarrow \pi^+\pi^-$ and continuum $\pi^+\pi^-$ production at $\sqrt{s} = 7$ TeV. The meaning of the lines is the same as in Fig. 8 (left panel).

effect of deviation from a constant is due to interference of photon-pomeron and pomeron-photon amplitudes. The interference is different for pp - and $p\bar{p}$ -collisions because proton and antiproton have opposite charges. A similar effect was first discussed in Ref. [25] for the exclusive production of J/ψ mesons. These correlations are rather different than those for the double-pomeron mechanism [12, 14] and could therefore be used for at least a partial separation of the two mechanisms. The absorption effects, see e.g. [14, 27], lead to extra decorrelation in azimuth compared to the Born-level results presented here.

Finally, in Fig. 14 we compare the photoproduction contribution with the double-pomeron/reggeon contribution one (for details see [11–13]). The absorption effects due to pp -interaction lead to huge damping of the cross section for pomeron-pomeron fusion and relatively small reduction of the cross section for the photoproduction mechanism. The dependence of absorption on $M_{\pi\pi}$ is quantified by the ratio of full and Born cross sections $\langle S^2(M_{\pi\pi}) \rangle = \frac{d\sigma^{Born+pp\text{-rescattering}}/dM_{\pi\pi}}{d\sigma^{Born}/dM_{\pi\pi}}$. We obtain $\langle S^2 \rangle \simeq 0.9$ for the photon-pomeron/reggeon contribution and $\langle S^2 \rangle \simeq 0.2$ for the double-pomeron/reggeon contribution. We observe that at midrapidities, imposing e.g. the cut $|\eta_\pi| < 0.9$, the photoproduction term could be visible in experiments.

In the present study we do not include interference effects between the photoproduction and the purely diffractive amplitudes. This goes beyond the scope of the present paper. We leave a detailed analysis of such effects for future studies when the diffractive mechanism with tensorial pomeron/reggeon will be discussed.

In Table 1 we have collected cross sections in μb for the exclusive $\pi^+\pi^-$ photoproduction contributions, see Figs. 1 and 2, for kinematical range of “ ρ^0 - mass window” $2m_\pi \leq M_{\pi\pi} \leq 1.5$ GeV and when some experimental cuts are imposed.

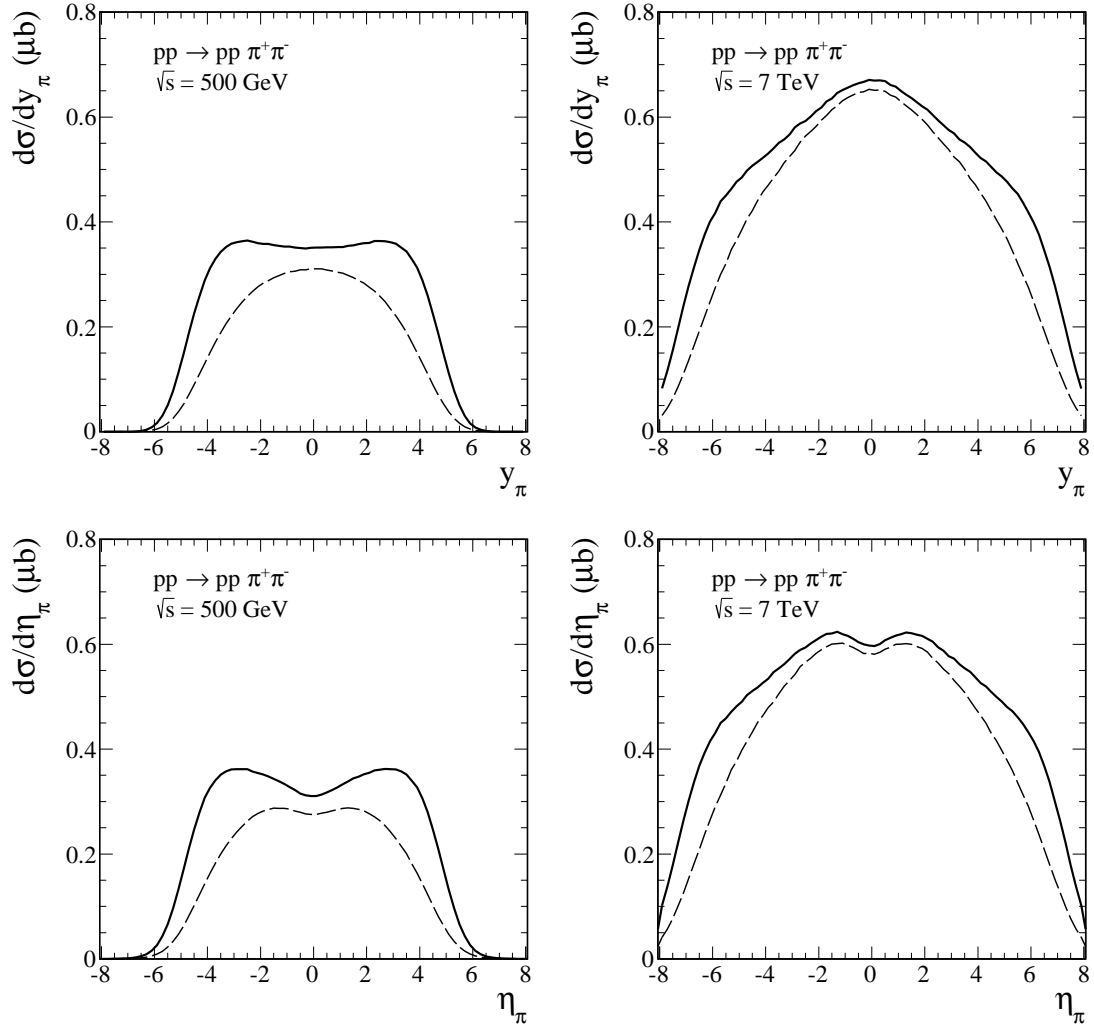


Figure 11. Rapidity (upper row) and pseudorapidity (lower row) distributions of pions produced in the photoproduction mechanism at $\sqrt{s} = 0.5$ and 7 TeV. The solid lines correspond to the pomeron and f_{2R} exchanges in the amplitudes while the dashed lines correspond to the pomeron exchange alone.

5 Conclusions and Outlook

In the present paper we have made first estimates of the ρ^0 resonance and the Drell-Söding contributions to the $pp \rightarrow pp\pi^+\pi^-$ and $p\bar{p} \rightarrow p\bar{p}\pi^+\pi^-$ reactions. We have shown several differential distributions in pion rapidities and transverse momenta as well as some observables related to final state protons. The photoproduction contribution constitutes several percent of the double-pomeron/reggeon contribution presented here in a simple Regge-like model, strongly depending on the invariant mass of the two-pion system. In the photoproduction contribution the rapidities of the two pions are strongly correlated and $y_{\pi^+} \approx y_{\pi^-}$. This is similar as for the double-pomeron/reggeon exchanges in the fully diffractive mechanism. The dependence on transverse momenta of pions is somewhat different for the two contri-

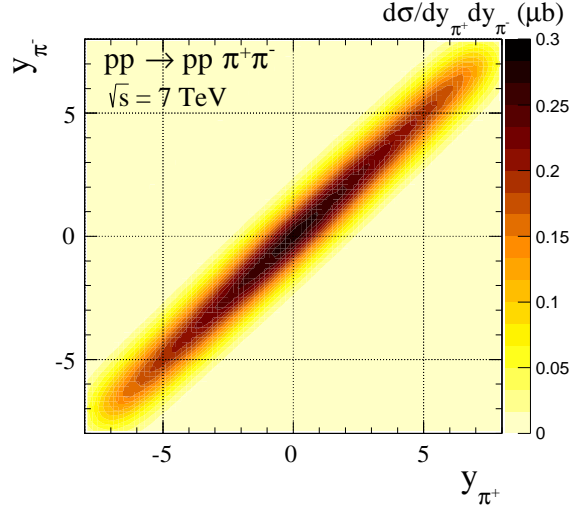


Figure 12. The correlation between the rapidities y_{π^+} and y_{π^-} for the photoproduction mechanism at $\sqrt{s} = 7$ TeV. Plotted is $d\sigma/dy_{\pi^+} dy_{\pi^-}$ in μb .

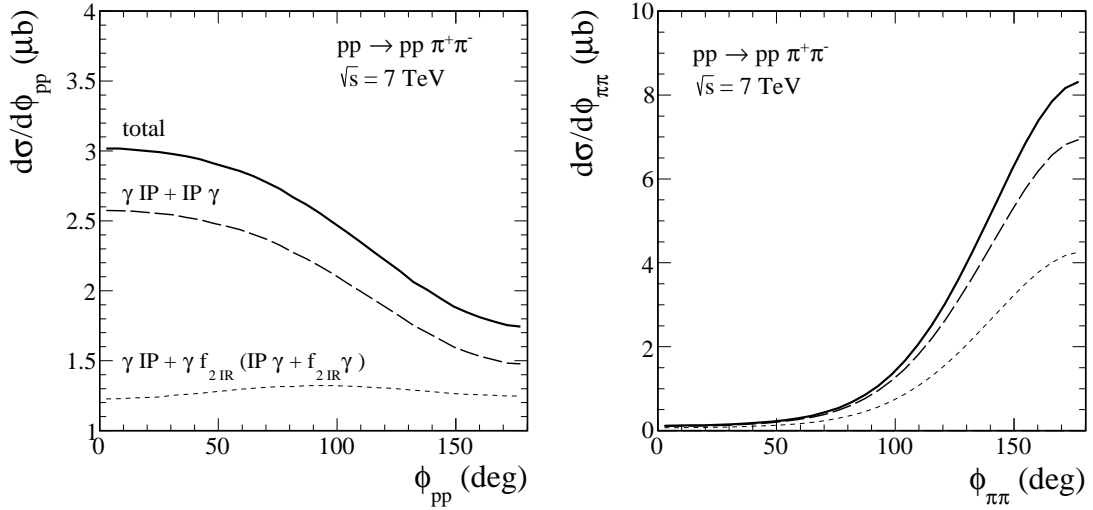


Figure 13. The distribution in azimuthal angle between the outgoing protons (left panel) and between the outgoing pions (right panel) for the central exclusive photoproduction at $\sqrt{s} = 7$ TeV. The solid lines correspond to the pomeron and f_{2IR} exchanges in the amplitudes while the long-dashed lines correspond to the pomeron exchange alone. The short-dashed line represents the contribution from $\gamma - \mathbb{P}/\mathbb{R}$ (or $\mathbb{P}/\mathbb{R} - \gamma$) exchange.

butions. Therefore, including transverse momentum dependent cuts changes the relative size of the photoproduction and double-pomeron/reggeon contributions.

Our cross section for $pp \rightarrow pp(\rho^0 \rightarrow \pi^+\pi^-)$ is slightly larger than for the $pp \rightarrow pp\rho^0$ with fixed sharp resonance mass. This is partly due to the different phase space for the four-body and three-body reactions.

The ρ^0 -photoproduction and purely diffractive contributions have different dependences

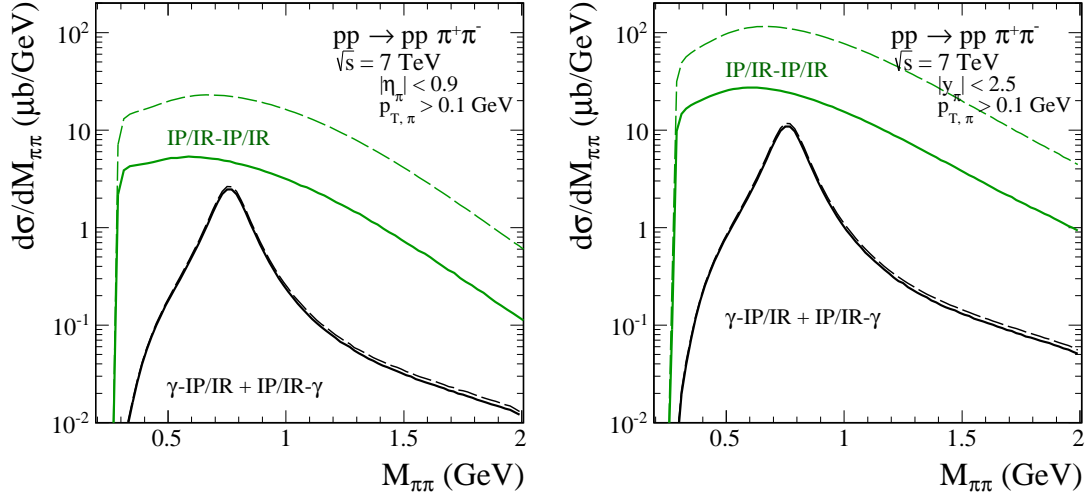


Figure 14. Two-pion invariant mass distributions at $\sqrt{s} = 7$ TeV with kinematical cuts specified in the figure. We show results for the double-pomeron/reggeon contribution calculated in the simple Lebiedowicz-Szczurek Regge-like model [11, 14] and from the photon-pomeron/reggeon contribution as discussed in the present paper, without (dashed lines) and with (solid lines) absorption effects due to the pp -interaction. The calculation of double-pomeron/reggeon contribution was done with the cut-off parameter $\Lambda_{off,E}^2 = 1.2$ GeV² in the off-shell pion form factors (see Section 2.3 of [14]).

\sqrt{s} , TeV	IP and f_{2R}	IP
0.2	2.22	1.36
0.5	3.38	2.31
1.96	5.77	4.51
7	7.80	6.64
0.2 (STAR cuts)	0.011	0.008
7 (ALICE cuts)	0.59	0.58
7 (CMS cuts)	2.61	2.53

Table 1. The integrated cross sections in μb for the central exclusive $\pi^+\pi^-$ production in pp collisions via the photoproduction mechanism without and with some typical experimental cuts. The line with $\sqrt{s} = 1.96$ TeV corresponds to the $p\bar{p}$ collision. The column “ IP and f_{2R} ” shows the resulting total cross sections from IP and f_{2R} exchanges, which include, of course, the interference term between the two components. The column “ IP ” shows results obtained for the IP exchange alone. In the calculations for the last three lines the following cuts were imposed: $|\eta_\pi| < 1.0$, $|\eta_{\pi\pi}| < 2.0$, $p_{\perp,\pi} > 0.15$ GeV, $0.005 < -t_1, -t_2 < 0.03$ GeV² at $\sqrt{s} = 200$ GeV (STAR cuts) while at the LHC energies $|y_\pi| < 2.5$, $p_{\perp,\pi} > 0.1$ GeV (CMS cuts) and $|\eta_\pi| < 0.9$, $p_{\perp,\pi} > 0.1$ GeV (ALICE cuts).

on the proton transverse momenta. This could be used to separate the ρ^0 contribution. Also azimuthal angle correlations between protons are quite different. One could separate the space in azimuthal angle into two regions: $\phi_{pp} < 90^\circ$ and $\phi_{pp} > 90^\circ$. The contribution of ρ^0 in the first region should be strongly enhanced for pp -collisions (this is not true for

$p\bar{p}$ -collisions). We therefore conclude that the measurement of forward/backward protons is crucial for a better understanding of the mechanism of the $pp \rightarrow pp\pi^+\pi^-$ reaction, see e.g. [8]. Both, the ALFA detector associated with the ATLAS main detector and particularly the TOTEM detector associated with the CMS main detector could be used to measure protons and pions in coincidence, see [10]. Also a cut on $\phi_{\pi\pi}$ could help to enhance the ρ^0 contribution.

In general, the ρ^0 and the whole photoproduction contribution could be obtained from partial wave analysis of the experimental results. Whether this is possible requires dedicated Monte Carlo studies.

We have also discussed the role of soft pp -rescattering corrections which lead to a shape deformation of differential distributions in contrast to the commonly used uniform factor known as gap survival factor. The absorptive corrections for photon induced reactions lead to about 10% reduction of the cross section. In the case of the photon-mediated contribution to central exclusive production of heavier mesons the effect is even larger, see e.g. [28].

In future work we shall present a calculation of the remaining processes leading to central exclusive $\pi^+\pi^-$ production in pp and $p\bar{p}$ collisions. These are, as already mentioned in the introduction, continuum $\pi^+\pi^-$ production via pomeron/reggeon - pomeron/reggeon fusion and $f_2(1270)$ production by the same mechanisms with the f_2 decaying into $\pi^+\pi^-$. All these reactions can be treated in the model for high-energy soft reactions presented in [16]. Concerning the photon-mediated processes discussed in the present paper one could also include the Pauli form factor in the proton's electromagnetic vertex as was done recently for exclusive production of J/ψ meson [28]. The effect of enhancements is expected only at large transverse momenta of the dipion pairs.

To summarise: using the tensor-pomeron approach we have treated the photon-mediated contributions to the central exclusive production of $\pi^+\pi^-$ in pp and $p\bar{p}$ collisions. The couplings involved are, in essence, known. Thus the predictions made with our model should be quite solid. This should give guidelines and a target to shoot at for experimentalists working on soft high-energy reactions at colliders.

Acknowledgments

We are indebted to C. Ewerz, M. Sauter, W. Schäfer, R. Schicker, and A. Schöning for useful discussions. The work of P.L. was supported by the Polish NCN grant DEC-2013/08/T/ST2/00165 (ETIUDA) and by the MNiSW grant no. IP2014 025173 “Iuventus Plus” as well as by the START fellowship from the Foundation for Polish Science. The work of A.S. was partially supported by the Polish NCN grant DEC-2011/01/B/ST2/04535 (OPUS) as well as by the Centre for Innovation and Transfer of Natural Sciences and Engineering Knowledge in Rzeszów.

References

- [1] **COMPASS** Collaboration, A. Austregesilo, *A Partial-Wave Analysis of Centrally Produced Two-Pseudoscalar Final States in pp Reactions at COMPASS*, *PoS Bormio2013* (2013) 014.
- [2] **STAR** Collaboration, J. Turnau, *Measurement of the Central Exclusive Production of pion pairs using tagged forward protons at the STAR detector at RHIC*, *PoS DIS2014* (2014) 098.
- [3] L. Adamczyk, W. Guryn, and J. Turnau, *Central exclusive production at RHIC*, [arXiv:1410.5752](#).
- [4] **CDF** Collaboration, M. Albrow, A. Świąch, and M. Żurek, *Exclusive Central $\pi^+\pi^-$ production in CDF*, [arXiv:1310.3839](#).
- [5] M. Albrow, J. Lewis, M. Żurek, A. Świąch, D. Lontkovskiy, I. Makarenko, and J. S. Wilson. The public note called *Measurement of Central Exclusive Hadron Pair Production in CDF* is available at http://www-cdf.fnal.gov/physics/new/qcd/GXG_14/webpage/.
- [6] **ALICE** Collaboration, R. Schicker, *Central Diffraction in ALICE*, [arXiv:1205.2588](#).
- [7] R. Schicker, *Diffraction production of mesons*, [arXiv:1410.6060](#).
- [8] R. Staszewski, P. Lebiedowicz, M. Trzebiński, J. Chwastowski, and A. Szczurek, *Exclusive $\pi^+\pi^-$ Production at the LHC with Forward Proton Tagging*, *Acta Phys.Polon.* **B42** (2011) 1861–1870, [[arXiv:1104.3568](#)].
- [9] D. d’Enterria. Private communication.
- [10] K. Österberg, *Potential of central exclusive production studies in high β^* runs at the LHC with CMS-TOTEM*, *Int.J.Mod.Phys.* **A29** (2014), no. 28 1446019.
- [11] P. Lebiedowicz and A. Szczurek, *Exclusive $pp \rightarrow pp\pi^+\pi^-$ reaction: From the threshold to LHC*, *Phys.Rev.* **D81** (2010) 036003, [[arXiv:0912.0190](#)].
- [12] P. Lebiedowicz, R. Pasechnik, and A. Szczurek, *Measurement of exclusive production of scalar χ_{c0} meson in proton-(anti)proton collisions via $\chi_{c0} \rightarrow \pi^+\pi^-$ decay*, *Phys.Lett.* **B701** (2011) 434–444, [[arXiv:1103.5642](#)].
- [13] P. Lebiedowicz and A. Szczurek, *$pp \rightarrow ppK^+K^-$ reaction at high energies*, *Phys.Rev.* **D85** (2012) 014026, [[arXiv:1110.4787](#)].
- [14] P. Lebiedowicz, *Exclusive reactions with light mesons: From low to high energies*. PhD thesis, IFJ PAN, 2014. The thesis is available at http://www.ifj.edu.pl/msd/rozprawy_dr/rozpr_Lebiedowicz.pdf.
- [15] P. Lebiedowicz, O. Nachtmann, and A. Szczurek, *Exclusive central diffractive production of scalar and pseudoscalar mesons; tensorial vs. vectorial pomeron*, *Annals Phys.* **344** (2014) 301–339, [[arXiv:1309.3913](#)].
- [16] C. Ewerz, M. Maniatis, and O. Nachtmann, *A Model for Soft High-Energy Scattering: Tensor Pomeron and Vector Odderon*, *Annals of Physics* **342** (2014) 31–77, [[arXiv:1309.3478](#)].
- [17] A. Bolz, C. Ewerz, M. Maniatis, O. Nachtmann, M. Sauter, and A. Schöning, *Photoproduction of $\pi^+\pi^-$ pairs in a model with tensor-pomeron and vector-odderon exchange*, [arXiv:1409.8483](#).
- [18] M. Sauter. A talk *Photoproduction of $\pi^+\pi^-$ pairs in a model with tensor-pomeron and vector-odderon exchange*, Low x Meeting, 17-21 June 2014, Kyoto, Japan.

- [19] S. D. Drell, *Production of Particle Beams at Very High Energies*, *Phys.Rev.Lett.* **5** (1960) 278–281.
- [20] S. D. Drell, *Peripheral Contributions to High-Energy Interaction Processes*, *Rev.Mod.Phys.* **33** (1961) 458–466.
- [21] P. Söding, *On the apparent shift of the rho meson mass in photoproduction*, *Phys.Lett.* **19** (1966) 702–704.
- [22] A. Szczurek and A. P. Szczepaniak, *Diffraction photoproduction of opposite-charge pseudoscalar meson pairs at high energies*, *Phys.Rev.* **D71** (2005) 054005, [[hep-ph/0410083](#)].
- [23] N. Armesto and A. H. Rezaeian, *Exclusive vector meson production at high energies and gluon saturation*, *Phys.Rev.* **D90** (2014) 054003, [[arXiv:1402.4831](#)].
- [24] G. S. dos Santos and M. V. T. Machado, *Light vector meson photoproduction in hadron-hadron and nucleus-nucleus collisions at the energies available at the CERN Large Hadron Collider*, [arXiv:1407.4148](#).
- [25] W. Schäfer and A. Szczurek, *Exclusive photoproduction of J/ψ in proton-proton and proton-antiproton scattering*, *Phys.Rev.* **D76** (2007) 094014, [[arXiv:0705.2887](#)].
- [26] A. Cisek, W. Schäfer, and A. Szczurek, *Exclusive photoproduction of ϕ meson in $\gamma p \rightarrow \phi p$ and $pp \rightarrow p\phi p$ reactions*, *Phys.Lett.* **B690** (2010) 168–174, [[arXiv:1004.0070](#)].
- [27] A. Cisek, P. Lebiedowicz, W. Schäfer, and A. Szczurek, *Exclusive production of ω meson in proton-proton collisions at high energies*, *Phys.Rev.* **D83** (2011) 114004, [[arXiv:1101.4874](#)].
- [28] A. Cisek, W. Schäfer, and A. Szczurek, *Exclusive photoproduction of charmonia in $\gamma p \rightarrow Vp$ and $pp \rightarrow pVp$ reactions within k_t -factorization approach*, [arXiv:1405.2253](#).
- [29] P. Lebiedowicz and A. Szczurek, *Exclusive $pp \rightarrow pp\pi^0$ reaction at high energies*, *Phys.Rev.* **D87** (2013) 074037, [[arXiv:1303.2882](#)].
- [30] P. Lebiedowicz and A. Szczurek, *Exclusive diffractive photon bremsstrahlung at the LHC*, *Phys.Rev.* **D87** (2013) 114013, [[arXiv:1302.4346](#)].
- [31] **STAR** Collaboration, C. Adler et al., *Coherent ρ^0 Production in Ultraperipheral Heavy Ion Collisions*, *Phys.Rev.Lett.* **89** (2002) 272302, [[nucl-ex/0206004](#)].
- [32] **STAR** Collaboration, B. I. Abelev et al., *ρ^0 Photoproduction in Ultraperipheral Relativistic Heavy Ion Collisions at $\sqrt{s_{NN}} = 200$ GeV*, *Phys.Rev.* **C77** (2008) 034910, [[arXiv:0712.3320](#)].
- [33] **STAR** Collaboration, B. I. Abelev et al., *Observation of Two-Source Interference in the Photoproduction Reaction $AuAu \rightarrow AuAu\rho^0$* , *Phys.Rev.Lett.* **102** (2009) 112301, [[arXiv:0812.1063](#)].
- [34] **STAR** Collaboration, G. Agakishiev et al., *ρ^0 Photoproduction in AuAu Collisions at $\sqrt{s_{NN}} = 62.4$ GeV with STAR*, *Phys.Rev.* **C85** (2012) 014910, [[arXiv:1107.4630](#)].
- [35] **for the ALICE** Collaboration, J. Nystrand, *Photonuclear Production of Vector Mesons in Ultra-Peripheral Pb-Pb Collisions at the LHC*, [arXiv:1408.0811](#).
- [36] G. Baur, K. Hencken, D. Trautmann, S. Sadovsky, and Y. Kharlov, *Coherent $\gamma\gamma$ and γA Interactions in Very Peripheral Collisions at Relativistic Ion Colliders*, *Phys.Rept.* **364** (2002) 359–450, [[hep-ph/0112211](#)].
- [37] C. A. Bertulani, S. R. Klein, and J. Nystrand, *Physics of Ultra-Peripheral Nuclear Collisions*, *Ann.Rev.Nucl.Part.Sci.* **55** (2005) 271–310, [[nucl-ex/0502005](#)].

- [38] A. J. Baltz, G. Baur, D. d’Enterria, L. Frankfurt, F. Gelis, et al., *The Physics of Ultraperipheral Collisions at the LHC*, *Phys.Rept.* **458** (2008) 1–171, [[arXiv:0706.3356](#)].
- [39] A. Donnachie, H. G. Dosch, P. V. Landshoff, and O. Nachtmann, *Pomeron physics and QCD*, *Camb.Monogr.Part.Phys.Nucl.Phys.Cosmol.* **19** (2002) 1–347.
- [40] **Particle Data Group** Collaboration, K. A. Olive et al., *Review of Particle Physics*, *Chin.Phys.* **C38** (2014) 090001.
- [41] B. Friman and M. Soyeur, *Photoproduction of vector mesons off nucleons near threshold*, *Nucl.Phys.* **A600** (1996) 477–490, [[nucl-th/9601028](#)].
- [42] J. M. Laget, *Photoproduction of vector mesons at large momentum transfer*, *Phys.Lett.* **B489** (2000) 313–318, [[hep-ph/0003213](#)].
- [43] Y. Oh, *Vector meson photoproduction processes near threshold*, *J.Korean Phys.Soc.* **43** (2003) S20–S26, [[nucl-th/0301011](#)].
- [44] Y. Oh and T.-S. H. Lee, *ρ meson photoproduction at low-energies*, *Phys.Rev.* **C69** (2004) 025201, [[nucl-th/0306033](#)].
- [45] F. Riek, R. Rapp, T.-S. H. Lee, and Y. Oh, *Medium Effects in ρ -Meson Photoproduction*, *Phys.Lett.* **B677** (2009) 116–120, [[arXiv:0812.0987](#)].
- [46] I. T. Obukhovskiy, A. Faessler, D. K. Fedorov, T. Gutsche, V. E. Lyubovitskij, V. G. Neudatchin, and L. L. Sviridova, *Quasielastic ρ^0 electroproduction on the proton at intermediate energy: Role of scalar and pseudoscalar meson exchange*, *Phys.Rev.* **D81** (2010) 013007, [[arXiv:0911.3074](#)].
- [47] **ZEUS** Collaboration, J. Breitweg et al., *Elastic and proton dissociative ρ^0 photoproduction at HERA*, *Eur.Phys.J.* **C2** (1998) 247–267, [[hep-ex/9712020](#)].
- [48] **ZEUS** Collaboration, J. Breitweg et al., *Measurement of diffractive photoproduction of vector mesons at large momentum transfer at HERA*, *Eur.Phys.J.* **C14** (2000) 213–238, [[hep-ex/9910038](#)].
- [49] **ZEUS** Collaboration, M. Derrick et al., *Measurement of total and partial photon proton cross-sections at 180 GeV center of mass energy*, *Z.Phys.* **C63** (1994) 391–408.
- [50] **ZEUS** Collaboration, M. Derrick et al., *Measurement of elastic ρ^0 photoproduction at HERA*, *Z.Phys.* **C69** (1995) 39–54, [[hep-ex/9507011](#)].
- [51] **ZEUS** Collaboration, M. Derrick et al., *Measurement of elastic ω photoproduction at HERA*, *Z.Phys.* **C73** (1996) 73–84, [[hep-ex/9608010](#)].
- [52] **H1** Collaboration, S. Aid et al., *Elastic photoproduction of ρ^0 mesons at HERA*, *Nucl.Phys.* **B463** (1996) 3–32, [[hep-ex/9601004](#)].
- [53] D. Melikhov, O. Nachtmann, V. Nikonov, and T. Paulus, *Masses and couplings of vector mesons from the pion electromagnetic, weak, and $\pi\gamma$ transition form factors*, *Eur.Phys.J.* **C34** (2004) 345–360, [[hep-ph/0311213](#)].
- [54] M. Poppe, *Exclusive Hadron Production in Two Photon Reactions*, *Int.J.Mod.Phys.* **A1** (1986) 545–668.
- [55] A. Szczurek and J. Speth, *Perturbative QCD versus pion exchange and hadronic FSI effects in the $\gamma\gamma \rightarrow \pi^+\pi^-$ reaction*, *Nucl.Phys.* **A728** (2003) 182–202, [[hep-ph/0207265](#)].

- [56] M. Kłusek-Gawenda and A. Szczurek, $\pi^+\pi^-$ and $\pi^0\pi^0$ pair production in photon-photon and in ultraperipheral ultrarelativistic heavy ion collisions, *Phys.Rev.* **C87** (2013), no. 5 054908, [[arXiv:1302.4204](#)].